A Tensor-Based Millimeter Wave Wideband Massive MIMO Channel Estimation Technique Using Uniform Planar Arrays

Junkang Hong, *Student Member, IEEE,* Jian Sun, *Member, IEEE,* Yubei He, *Student Member, IEEE,* Wensheng Zhang, *Member, IEEE,* and Cheng-Xiang Wang, *Fellow, IEEE*

***Abstract*—This letter focuses on the millimeter wave (mmWave) wideband directional channel estimation problem for a channel sounding system based on massive multiple-input multiple-output (MIMO). The received signals of the wideband pilot sequence are concatenated into a low-rank third-order tensor. By leveraging the Vandermonde structure of the factor matrices which construct the signal tensor, an algebra-based CANDECOMP/PARAFAC (CP) decomposition method is used to reconstruct the factor matrices, from which the channel parameters are estimated by a two-dimensional (2-D) correlation-based search method and refined by the Nelder-Mead simplex (NMS) algorithm. With the designed Kronecker-structured precoder and combiner, the 2-D search method can be simplified to a 1-D search method. A channel path number estimation method by analyzing the singular values of the expanded signal tensor is also proposed. Simulation results with the synthesized channel data illustrate that the proposed algorithm can obtain high estimation accuracy.**

***Index Terms*—MmWave communication, channel estimation, massive MIMO, tensor decomposition, path number estimation.**

I. Introduction

MMWAVE communication technology has been widely considered one of the most prospective technologies in the fifth-generation (5G) and sixth-generation (6G) wireless communication systems. By exploiting the vast bandwidth, mmWave communication can achieve a peak rate of 20 Gbps [1]. However, the issues faced by mmWave signals, such as high path loss and susceptibility to obstructions, have limited the development and application of mmWave communication technology. Therefore, massive MIMO is introduced to provide flexible beamforming, enhance the spatial multiplexing capability, and overcome high path loss [2]. The orthogonal frequency-division multiplexing (OFDM) technology is also adopted to improve spectrum utilization and overcome frequency selective fading. To reduce hardware costs effectively, hybrid beamforming (HBF) is applied. However, the compressed signal structure makes channel estimation challenging for massive MIMO systems adopting HBF technology. Accurate channel state information (CSI) is required for channel sounding and modeling. We expect to use the same mmWave massive MIMO-OFDM communication front-end system as a channel sounder to conduct channel measurements. Good channel estimation schemes are to be developed for such channel sounders.

Most existing channel estimation schemes for mmWave channel sounding consider uniform linear arrays (ULAs) for both transmitter (Tx) and receiver (Rx). A space-alternating generalized expectation-maximization (SAGE) based channel estimation scheme was proposed in [3], where an iterative cancellation method was used to initialize the channel parameters. By exploiting the sparsity structure of the mmWave channel in both time and frequency domains, schemes based on compressed sensing (CS) theory transformed the mmWave channel estimation into a sparse recovery problem [4]. As a powerful mathematical tool, tensors can hold the structure of signals, and channel parameters can be restored by tensor decomposition. In [5]–[7], the received signals were converted into low-rank tensors, and the parameters were extracted by tensor decomposition. A channel estimation scheme using an alternating least-squares (ALS) based CP decomposition was proposed in [5]. However, our simulation found it often cannot converge to the vicinity of the true value, thus failing to achieve good performance. Reference [6], [7] considered channel estimation for 3-D massive MIMO systems equipped with uniform planar arrays (UPAs), namely, it can estimate azimuth and elevation angles at both ends. A non-iterative channel estimation scheme based on tensor decomposition and rotational invariance techniques for mmWave channel tensors with Vandermonde factor matrices was proposed in [6]. However, the Vandermonde structure was required for both the precoder and combiner, which limited the application of this scheme. Similarly, by leveraging the Vandermonde structure of the factor matrices, [7] proposed to reconstruct the signal subspaces using the tensor train (TT) decomposition. Although the proposed scheme can improve the estimation accuracy, the computational complexity was also increased.

Our previous work [8] used an algebra-based method to conduct CP decomposition, which also utilizes the Vandermonde structure of the signal tensor. The method has been proven to increase the stability and accuracy of channel estimation. This letter extends the approach for channel estimation of mmWave wideband 3-D massive MIMO-OFDM systems and improves the angle estimation algorithm. Different from [6] and [7] converting the received signals into a high-order tensor, we rearrange the received signals into simpler third-order tensors and use the Kronecker structure of the factor matrices to reduce computational complexity. We refine the initial estimated angles by the NMS algorithm to achieve higher estimation accuracy. A highly reliable singular value-based channel path number estimation method is also proposed

This work was supported by the National Natural Science Foundation of China (NSFC) under Grant 62071276 and the National Key R&D Program of China under Grant 2022YFF0604903.

Junkang Hong, Jian Sun (Corresponding author), Yubei He, and Wensheng Zhang (Corresponding author) are with the Shandong Provincial Key Lab of Wireless Communication Technologies, School of Information Science and Engineering, Shandong University, Qingdao 266237, China (e-mail: 202112679@mail.sdu.edu.cn; sunjian@sdu.edu.cn; heyubei@126.com; zhangwsh@sdu.edu.cn). Cheng-Xiang Wang is with the National Mobile Communications Research Laboratory, School of Information Science and Engineering, Southeast University, Nanjing, Jiangsu 210096, China, and also with the Purple Mountain Laboratories, Nanjing 211111, China (e-mail:chxwang@seu.edu.cn).

for the case of unknown channel path numbers.

Notations: Bold lowercase letters, bold capital letters, and Euler script letters denote vectors, matrices, and tensors, respectively. Superscript $(\cdot)^T$,$(\cdot)^H$,$(\cdot)^{-1}$,$(\cdot)^*$, and $(\cdot)^\dagger$ denote the transpose, conjugate transpose, inverse, conjugate, and pseudo inverse, respectively. $\circ$, $\odot$, and $\otimes$ represent the outer product, Khatri-Rao product, and Kronecker product, respectively. $[\mathbf{X}]_i$ and $[\mathbf{X}]_{i:j}$ denote the ith row of $\mathbf{X}$ and the submatrix from the ith to the jth rows of $\mathbf{X}$, respectively. $\mathrm{D}(\mathbf{x})$ denotes the diagonal matrix formed by $\mathbf{x}$. $\mathbf{I}_x$ denotes the identity matrix of size x. $|\cdot|$ and $||\cdot||_2$ denote the absolute value and 2-norm, respectively. $\hat{\mathbf{X}}$ represents the estimation of $\mathbf{X}$.

II. SYSTEM MODEL

A. Wideband mmWave 3-D massive MIMO channel

As shown in Fig. 1, we consider a mmWave massive MIMO-OFDM system with UPA antennas of size $M(M = M_1 \times M_2)$ and $N(N = N_1 \times N_2)$ equipped at the Tx and Rx, respectively. Both UPAs are placed face to face on the yoz plane. The HBF technique is adopted, but only analog beamforming is utilized for channel sounding here. We assume that the Rx is configured with N_{RF} RF chains, and only one RF chain is used at the Tx to avoid interference. Owing to the sparsity structure of the mmWave channel, the wideband, i.e., frequency-selective mmWave 3-D massive MIMO channel, can be described by the geometry-based stochastic channel model, which is the superposition of L scattering paths [9]. The channel is considered constant during the channel sounding. Suppose that K subcarriers are used for the OFDM pilot transmission, the channel matrix $\mathbf{H}_k \in \mathbb{C}^{N\times M}, k = 0, 1, \ldots, K-1$ on the kth subcarrier is

$$\mathbf{H}_k = \sum_{l=1}^{L} \alpha_l e^{-j\frac{2\pi k\tau_l}{K}} \mathbf{a}_R(\theta_l, \phi_l)\mathbf{a}_T^H(\vartheta_l, \varphi_l) \tag{1}$$

where α_l, τ_l, θ_l/ϕ_l, and ϑ_l/φ_l denote the complex path gain, delay normalized by the sampling interval, azimuth/elevation angle of arrival (AoA), and azimuth/elevation angle of departure (AoD) of the lth path, respectively. According to the UPA geometry, we define $\mathbf{a}_{Ry}(\theta_l, \phi_l) = e^{j2\pi\frac{d}{\lambda}sin\theta_l sin\phi_l \mathbf{n}_1}$, $\mathbf{a}_{Rz}(\phi_l) = e^{j2\pi\frac{d}{\lambda}cos\phi_l \mathbf{n}_2}$, $\mathbf{a}_{Ty}(\vartheta_l, \varphi_l) = e^{j2\pi\frac{d}{\lambda}sin\vartheta_l sin\varphi_l \mathbf{m}_1}$, and $\mathbf{a}_{Tz}(\varphi_l) = e^{j2\pi\frac{d}{\lambda}cos\varphi_l \mathbf{m}_2}$, where $\mathbf{n}_1 = [0, 1, \ldots, N_1-1]^T$, $\mathbf{n}_2 = [0, 1, \ldots, N_2 - 1]^T$, $\mathbf{m}_1 = [0, 1, \ldots, M_1 - 1]^T$, and $\mathbf{m}_2 = [0, 1, \ldots, M_2 - 1]^T$. λ denotes the carrier wavelength, and $d = \frac{\lambda}{2}$ denotes the antenna spacing. The steering vectors $\mathbf{a}_R(\theta_l, \phi_l) \in \mathbb{C}^{N\times 1}$ and $\mathbf{a}_T(\vartheta_l, \varphi_l) \in \mathbb{C}^{M\times 1}$ can be written as

$$\begin{aligned} \mathbf{a}_R(\theta_l, \phi_l) &= \mathbf{a}_{Ry}(\theta_l, \phi_l) \otimes \mathbf{a}_{Rz}(\phi_l) \\ \mathbf{a}_T(\vartheta_l, \varphi_l) &= \mathbf{a}_{Ty}(\vartheta_l, \varphi_l) \otimes \mathbf{a}_{Tz}(\varphi_l). \end{aligned} \tag{2}$$

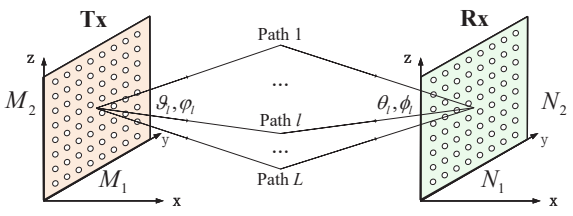

Fig. 1. Wideband mmWave 3-D channel for massive MIMO-OFDM system with UPAs.

B. Signal model

Assume that a pilot sequence of length N_X is sent by Tx for channel sounding. Each pilot symbol $s_p, p = 1, 2, \ldots, N_X$ is mapped onto the antennas at the Tx by the precoder $\mathbf{f}_p \in \mathbb{C}^{M\times 1}$ and modulated by the subcarrier modulation symbol x_k onto kth subcarrier. s_p and x_k are symbols of pseudo-random sequences with values of ± 1. N_{RF} RF chains are used to receive the pilot sequence parallelly. N_{RF} OFDM symbols will be obtained from the N_{RF} RF chains in a single time slot for each transmitted OFDM symbol. A combiner $\mathbf{W}_t \in \mathbb{C}^{N\times N_{RF}}, t = 1, 2, \ldots .T$ is employed to combine the received signal block in the tth time slot. Varying $T = \frac{N_Y}{N_{RF}}$ time slots, N_Y OFDM symbols will be received. After removing the cyclic prefix and FFT operation, the received signal of the pth pilot symbol in the tth time slot on the kth subcarrier is written as

$$\tilde{\mathbf{y}}_{k,p,t} = \mathbf{W}_t^H \mathbf{H}_k \mathbf{f}_p x_k s_p + \tilde{\boldsymbol{n}}_{k,p,t} \in \mathbb{C}^{N_{RF}\times 1} \tag{3}$$

where $\tilde{\boldsymbol{n}}_{k,p,t}$ is the additive white Gaussian noise vector. Since s_p and x_k are known at the Rx, they can be removed from Eq.(3). Then we have

$$\mathbf{y}_{k,p,t} = \mathbf{W}_t^H \mathbf{H}_k \mathbf{f}_p + \boldsymbol{n}_{k,p,t} \in \mathbb{C}^{N_{RF}\times 1} \tag{4}$$

where $\mathbf{y}_{k,p,t} = x_k s_p \tilde{\mathbf{y}}_{k,p,t}$ and $\boldsymbol{n}_{k,p,t} = x_k s_p \tilde{\boldsymbol{n}}_{k,p,t}$. $\boldsymbol{n}_{k,p,t}$ is also an additive white Gaussian noise vector as the variance and independence of noise at different subcarriers, receiving antennas, and time slots are unchanged. Combining the received signals in T time slots, we have

$$\mathbf{y}_{k,p} = \mathbf{W}^H \mathbf{H}_k \mathbf{f}_p + \boldsymbol{n}_{k,p} \tag{5}$$

where $\mathbf{y}_{k,p} = [\mathbf{y}_{k,p,1}^T, \mathbf{y}_{k,p,2}^T, \ldots, \mathbf{y}_{k,p,T}^T]^T \in \mathbb{C}^{N_Y\times 1}$, $\boldsymbol{n}_{k,p} = [\boldsymbol{n}_{k,p,1}^T, \boldsymbol{n}_{k,p,2}^T, \ldots, \boldsymbol{n}_{k,p,T}^T]^T \in \mathbb{C}^{N_Y\times 1}$, and $\mathbf{W} = [\mathbf{W}_1, \mathbf{W}_2, \ldots, \mathbf{W}_T] \in \mathbb{C}^{N\times N_Y}$. The received signals for the pilot sequence of length N_X on the kth subcarrier are given by

$$\mathbf{Y}_k = \mathbf{W}^H \mathbf{H}_k \mathbf{F} + \boldsymbol{N}_k \tag{6}$$

where $\mathbf{Y}_k = [\mathbf{y}_{k,1}, \mathbf{y}_{k,2}, \ldots, \mathbf{y}_{k,N_X}] \in \mathbb{C}^{N_Y\times N_X}$, $\mathbf{F} = [\mathbf{f}_1, \mathbf{f}_2, \ldots, \mathbf{f}_{N_X}] \in \mathbb{C}^{M\times N_X}$, and $\boldsymbol{N}_k = [\boldsymbol{n}_{k,1}, \boldsymbol{n}_{k,2}, \ldots, \boldsymbol{n}_{k,N_X}] \in \mathbb{C}^{N_Y\times N_X}$. After stacking $\tilde{\mathbf{Y}}_k$ for all K subcarriers, we can concatenate the received signals into a low-rank tensor $\mathcal{Y} \in \mathbb{C}^{N_Y\times N_X\times K}$ due to the sparsity structure of the mmWave channel

$$\mathcal{Y} = \sum_{l=1}^{L} \tilde{\mathbf{a}}_R(\theta_l, \phi_l) \circ \tilde{\mathbf{a}}_T(\vartheta_l, \varphi_l) \circ \mathbf{g}(\tau_l) + \mathcal{N} \tag{7}$$

where $\mathcal{N} \in \mathbb{C}^{N_Y\times N_X\times K}$ is the noise tensor, $\tilde{\mathbf{a}}_R(\theta_l, \phi_l) = \alpha_l \mathbf{W}^H \mathbf{a}_R(\theta_l, \phi_l) \in \mathbb{C}^{N_Y\times 1}$, $\tilde{\mathbf{a}}_T(\vartheta_l, \varphi_l) = \mathbf{F}^T \mathbf{a}_T^*(\vartheta_l, \varphi_l) \in \mathbb{C}^{N_X\times 1}$, and $\mathbf{g}(\tau_l) = [1, e^{-j\frac{2\pi\tau_l}{K}}, \ldots, e^{-j\frac{2\pi(K-1)\tau_l}{K}}]^T \in \mathbb{C}^{K\times 1}$. By CP decomposition, the third-order tensor can be decomposed as [10]

$$\mathcal{Y} = [\![\mathbf{A}^{(1)}, \mathbf{A}^{(2)}, \mathbf{A}^{(3)}]\!] + \mathcal{N} = \tilde{\mathcal{Y}} + \mathcal{N} \tag{8}$$

where $[\![\cdot]\!]$ represents the CP decomposition operator, $\tilde{\mathcal{Y}}$ denotes the received noiseless signal tensor, and $\mathbf{A}^{(1)} \in \mathbb{C}^{N_Y\times L}$, $\mathbf{A}^{(2)} \in \mathbb{C}^{N_X\times L}$, and $\mathbf{A}^{(3)} \in \mathbb{C}^{K\times L}$ are factor matrices of $\tilde{\mathcal{Y}}$, which are formed by

$$\begin{aligned} \mathbf{A}^{(1)} &= [\tilde{\mathbf{a}}_R(\theta_1, \phi_1), \tilde{\mathbf{a}}_R(\theta_2, \phi_2), \ldots, \tilde{\mathbf{a}}_R(\theta_L, \phi_L)] \\ \mathbf{A}^{(2)} &= [\tilde{\mathbf{a}}_T(\vartheta_1, \varphi_1), \tilde{\mathbf{a}}_T(\vartheta_2, \varphi_2), \ldots, \tilde{\mathbf{a}}_T(\vartheta_L, \varphi_L)] \\ \mathbf{A}^{(3)} &= [\mathbf{g}(\tau_1), \mathbf{g}(\tau_2), \ldots, \mathbf{g}(\tau_L)]. \end{aligned} \tag{9}$$

Note that $\mathbf{A}^{(3)}$ is a Vandermonde matrix that can be generated by $\mathbf{z} = [e^{\frac{-j2\pi\tau_1}{K}}, e^{\frac{-j2\pi\tau_2}{K}}, \ldots, e^{\frac{-j2\pi\tau_L}{K}}]$.

We can design $\mathbf{F}$ and $\mathbf{W}$ to have Kronecker structure as

$$\mathbf{F} = \mathbf{T}_1 \otimes \mathbf{T}_2, \qquad \mathbf{W} = \mathbf{R}_1 \otimes \mathbf{R}_2 \tag{10}$$

where $\mathbf{T}_1 \in \mathbb{C}^{M_1 \times J_1}$, $\mathbf{T}_2 \in \mathbb{C}^{M_2 \times J_2}$, $\mathbf{R}_1 \in \mathbb{C}^{N_1 \times I_1}$, and $\mathbf{R}_2 \in \mathbb{C}^{N_2 \times I_2}$ with $J_1 \times J_2 = N_X$ and $I_1 \times I_2 = N_Y$, each element in $\mathbf{T}_1, \mathbf{T}_2, \mathbf{R}_1$, and $\mathbf{R}_2$ is a uniformly distributed random value drawn from a unit circle. Define $\tilde{\mathbf{a}}_{Ry}(\theta_l, \phi_l) = \alpha_l \mathbf{R}_1^H \mathbf{a}_{Ry}(\theta_l, \phi_l)$, $\tilde{\mathbf{a}}_{Rz}(\phi_l) = \mathbf{R}_2^H \mathbf{a}_{Rz}(\phi_l)$, $\tilde{\mathbf{a}}_{Ty}(\vartheta_l, \varphi_l) = \mathbf{T}_1^T \mathbf{a}_{Ty}^*(\vartheta_l, \varphi_l)$, and $\tilde{\mathbf{a}}_{Tz}(\varphi_l) = \mathbf{T}_2^T \mathbf{a}_{Tz}^*(\varphi_l)$, by combining (2), (10), and (A.1) in Appendix A, we obtain

$$\begin{aligned} \tilde{\mathbf{a}}_R(\theta_l, \phi_l) &= \tilde{\mathbf{a}}_{Ry}(\theta_l, \phi_l) \otimes \tilde{\mathbf{a}}_{Rz}(\phi_l) \\ \tilde{\mathbf{a}}_T(\vartheta_l, \varphi_l) &= \tilde{\mathbf{a}}_{Ty}(\vartheta_l, \varphi_l) \otimes \tilde{\mathbf{a}}_{Tz}(\varphi_l). \end{aligned} \tag{11}$$

The Kronecker structure for each column of the factor matrices $\mathbf{A}^{(1)}$ and $\mathbf{A}^{(2)}$ can be used to reduce the computational complexity, which will be discussed in the next section.

III. CHANNEL ESTIMATION METHODS

A. Tensor-based Channel Estimation Algorithm

A fast non-iterative algebra-based method is presented in [11]. Different from the common ALS-based method, the CP decomposition is solved by exploiting the Vandermonde structure of $\mathbf{A}^{(3)}$. The noiseless signal tensor $\tilde{\mathcal{Y}}$ is used to develop our channel estimation algorithm that reveals the key insights. $\tilde{\mathcal{Y}}$ should be replaced by $\mathcal{Y}$ in the presence of noise.

Spatial smoothing is a technique to overcome the rank deficient problem, which can improve the estimation accuracy and uniqueness condition [12]. The Vandermonde structure of $\mathbf{A}^{(3)}$ makes spatial smoothing over $\mathbf{A}^{(3)}$ possible. Unfolding $\tilde{\mathcal{Y}}$ in the first dimension as $\tilde{\mathbf{Y}}_{(1)} = \mathbf{A}^{(1)} \left(\mathbf{A}^{(3)} \odot \mathbf{A}^{(2)}\right)^T \in \mathbb{C}^{N_Y \times N_X K}$. Defining a selection matrix $\mathbf{X}_i, i = 1, 2, \ldots, I_0$ as $\mathbf{X}_i = [\ \mathbf{0}_{J_0 \times (i-1)} \quad \mathbf{I}_{J_0} \quad \mathbf{0}_{J_0 \times (I_0 - i)}\ ] \in \mathbb{C}^{J_0 \times K}$, where I_0 and J_0 subject to $I_0 + J_0 = K + 1$. $\mathbf{X}_i$ is used to select the submatrix of $\mathbf{A}^{(3)}$, i.e., $\mathbf{X}_i \mathbf{A}^{(3)} = [\mathbf{A}^{(3)}]_{i:i+J_0-1}$. By (A.2), the spatial smoothing of $\tilde{\mathbf{Y}}_{(1)}$ is given by [8], [11], [12]

$$\tilde{\mathbf{Y}}^s = (\mathbf{A}^{(J_0,3)} \odot \mathbf{A}^{(2)})(\mathbf{A}^{(I_0,3)} \odot \mathbf{A}^{(1)})^T \in \mathbb{C}^{J_0 N_X \times I_0 N_Y} \tag{12}$$

where $\mathbf{A}^{(J_0,3)}$ and $\mathbf{A}^{(I_0,3)}$ denote $[\mathbf{A}^{(3)}]_{1:J_0}$ and $[\mathbf{A}^{(3)}]_{1:I_0}$, respectively. Assuming L is known, we take truncated singular value decomposition (SVD) over $\tilde{\mathbf{Y}}^s$ and get

$$\tilde{\mathbf{Y}}^s = \mathbf{U} \mathbf{\Sigma} \mathbf{V}^H \tag{13}$$

where $\mathbf{U} \in \mathbb{C}^{J_0 N_X \times L}$, $\mathbf{\Sigma} \in \mathbb{C}^{L \times L}$, and $\mathbf{V} \in \mathbb{C}^{I_0 N_Y \times L}$. $\mathbf{\Sigma}$ is a diagonal matrix with the diagonal element being the largest L singular values of $\tilde{\mathbf{Y}}^s$, $\mathbf{U}$ and $\mathbf{V}$ are left and right singular matrices corresponding to these singular values. There must exist a nonsingular matrix $\mathbf{M} \in \mathbb{C}^{L \times L}$ connecting these two signal space expressions (12) and (13), which satisfies

$$\begin{aligned} \mathbf{U}\mathbf{M} &= (\mathbf{A}^{(J_0,3)} \odot \mathbf{A}^{(2)}) \\ \mathbf{V}^* \mathbf{\Sigma} (\mathbf{M}^{-1})^T &= (\mathbf{A}^{(I_0,3)} \odot \mathbf{A}^{(1)}). \end{aligned} \tag{14}$$

By the Vandermonde structure of $\mathbf{A}^{(3)}$ and (A.3), we have

$$([\mathbf{A}^{(J_0,3)}]_{2:J_0} \odot \mathbf{A}^{(2)}) = ([\mathbf{A}^{(J_0,3)}]_{1:J_0-1} \odot \mathbf{A}^{(2)})\mathbf{Z} \tag{15}$$

where $\mathbf{Z} = \mathrm{D}(\mathbf{z})$. We define $\mathbf{U}_1 = [\mathbf{U}]_{1:(J_0-1)N_X}$ and $\mathbf{U}_2 = [\mathbf{U}]_{N_X+1:J_0 N_X}$. From (14) and (15), we can obtain

$$\mathbf{U}_1^\dagger \mathbf{U}_2 = \mathbf{M}\mathbf{Z}\mathbf{M}^{-1} \triangleq \tilde{\mathbf{Z}}. \tag{16}$$

Eq.(16) is a similarity transformation. Therefore, the eigenvalue of $\tilde{\mathbf{Z}}$ contains the delays $\{\tau_l\}_{l=1}^L$. We decompose the $\tilde{\mathbf{Z}}$ by eigenvalue decomposition (EVD) and have

$$\tilde{\mathbf{Z}} = \mathbf{Q} \mathbf{\Gamma} \mathbf{Q}^{-1} \tag{17}$$

where $\mathbf{\Gamma} = \mathrm{D}([\gamma_1, \gamma_2, \ldots, \gamma_L])$. Comparing (16) and (17), there must exist a permutation matrix $\mathbf{\Pi}$ and a diagonal scaling matrix $\mathbf{\Delta}$ linking $\mathbf{M}$, $\mathbf{Q}$, $\mathbf{\Gamma}$, and $\mathbf{Z}$, i.e., $\mathbf{Q} = \mathbf{M}\mathbf{\Delta}\mathbf{\Pi}$, and $[\gamma_1, \gamma_2, \ldots, \gamma_L] = \mathbf{z}\mathbf{\Pi}$. Then the delays are estimated by $\hat{\tau}_l = \frac{-K \arg(\gamma_l)}{2\pi}$, where $\arg(\gamma_l)$ denotes the phase angle of γ_l. From the estimated delay, we construct a new factor matrix $\mathbf{B}^{(3)} = [\mathbf{g}(\hat{\tau}_1), \mathbf{g}(\hat{\tau}_2), \ldots, \mathbf{g}(\hat{\tau}_L)]$ following the context below (7). As $\hat{\tau}_l, l = 1, \ldots, L$ are permutation of the true delay τ_l, $\mathbf{B}^{(3)}$ is the permutated form of $\mathbf{A}^{(3)}$, i.e., $\mathbf{B}^{(3)} = \mathbf{A}^{(3)}\mathbf{\Pi}$. Therefore, (14) can be rewritten as $\mathbf{U}\mathbf{Q}\mathbf{\Pi}^{-1}\mathbf{\Delta}^{-1} = (\mathbf{B}^{(J_0,3)}\mathbf{\Pi}^{-1}) \odot \mathbf{A}^{(2)}$ and $\mathbf{V}^*\mathbf{\Sigma}((\mathbf{Q}\mathbf{\Pi}^{-1}\mathbf{\Delta}^{-1})^{-1})^T = (\mathbf{B}^{(I_0,3)}\mathbf{\Pi}^{-1}) \odot \mathbf{A}^{(1)}$. By using (A.3) and (A.4), we obtain

$$\mathbf{U}\mathbf{Q} = \mathbf{B}^{(J_0,3)} \odot \mathbf{B}^{(2)} \tag{18a}$$

$$\mathbf{V}^*\mathbf{\Sigma}(\mathbf{Q}^{-1})^T = \mathbf{B}^{(I_0,3)} \odot \mathbf{B}^{(1)} \tag{18b}$$

where $\mathbf{B}^{(1)} = \mathbf{A}^{(1)}\mathbf{\Delta}^{-1}\mathbf{\Pi}$ and $\mathbf{B}^{(2)} = \mathbf{A}^{(2)}\mathbf{\Delta}\mathbf{\Pi}$, respectively. $[\![\mathbf{B}^{(1)}, \mathbf{B}^{(2)}, \mathbf{B}^{(3)}]\!]$ is another form of essential unique CP solution of $\tilde{\mathcal{Y}}$, which is proven in [8], [11] and, [12].

Next, the factor matrices $\mathbf{B}^{(1)}$ and $\mathbf{B}^{(2)}$ are reconstructed column by column. Let $\mathbf{b}_l^{(2)}$ and $\mathbf{b}_l^{(J_0,3)}$ denote the lth column of $\mathbf{B}^{(2)}$ and $\mathbf{B}^{(J_0,3)}$, respectively. Due to $\mathbf{b}_l^{(3)} = \mathbf{g}(\hat{\tau}_l)$, we have $\mathbf{b}_l^{(J_0,3)H}\mathbf{b}_l^{(J_0,3)} = J_0$. By (18a), we obtain $\mathbf{b}_l^{(J_0,3)} \otimes \mathbf{b}_l^{(2)} = \mathbf{U}\mathbf{q}_l$, where $\mathbf{q}_l$ is the lth column of $\mathbf{Q}$. Therefore, according to (A.1), $\mathbf{b}_l^{(2)} = \mathbf{I}_1 \otimes \mathbf{b}_l^{(2)}$ can be expanded as

$$\mathbf{b}_l^{(2)} = \left(\frac{\mathbf{b}_l^{(J_0,3)H}}{J_0} \otimes \mathbf{I}_{N_X}\right) \mathbf{U}\mathbf{q}_l. \tag{19}$$

Let $\mathbf{b}_l^{(1)}$ and $\mathbf{q}_l^{(inv)}$ denote the lth column of $\mathbf{B}^{(1)}$ and $(\mathbf{Q}^{-1})^T$, respectively. Similar to (19), by expanding $\mathbf{b}_l^{(1)} = \mathbf{I}_1 \otimes \mathbf{b}_l^{(1)}$ and leveraging (18b), we have

$$\mathbf{b}_l^{(1)} = \left(\frac{\mathbf{b}_l^{(I_0,3)H}}{I_0} \otimes \mathbf{I}_{N_Y}\right) \mathbf{V}^*\mathbf{\Sigma}\mathbf{q}_l^{(inv)}. \tag{20}$$

The factor matrices $\mathbf{B}^{(1)}, \mathbf{B}^{(2)}$, and $\mathbf{B}^{(3)}$ have the same permutation matrix $\mathbf{\Pi}$, such unknown permutation ambiguity only changes the order of reconstruction results. The AoAs and AoDs can be estimated by a correlation-based method

$$\begin{aligned} (\hat{\theta}_l, \hat{\phi}_l) &= \underset{\theta_l, \phi_l}{\mathrm{argmax}} \frac{|\mathbf{b}_l^{(1)H}(\mathbf{W}^H \mathbf{a}_R(\theta_l, \phi_l))|}{\|\mathbf{b}_l^{(1)}\|_2 \|(\mathbf{W}^H \mathbf{a}_R(\theta_l, \phi_l))\|_2} \\ (\hat{\vartheta}_l, \hat{\varphi}_l) &= \underset{\vartheta_l, \varphi_l}{\mathrm{argmax}} \frac{|\mathbf{b}_l^{(2)H}(\mathbf{F}^T \mathbf{a}_T^*(\vartheta_i, \varphi_l))|}{\|\mathbf{b}_l^{(2)}\|_2 \|(\mathbf{F}^T \mathbf{a}_T^*(\vartheta_i, \varphi_l))\|_2} \end{aligned} \tag{21}$$

where normalization operations eliminate the scaling ambiguity. A 2-D search method is adopted to find the coarse angles, and then the results are refined by the NMS algorithm [13].

Till now, the channel parameters $\{\hat{\tau}_l, \hat{\theta}_l, \hat{\phi}_l, \hat{\vartheta}_l, \hat{\varphi}_l\}_{l=1}^L$ are sequentially obtained. We reconstruct the factor matrices as

$$\begin{aligned} \hat{\mathbf{B}}^{(1)} &= \mathbf{W}^H[\mathbf{a}_R(\hat{\theta}_1, \hat{\phi}_1), \mathbf{a}_R(\hat{\theta}_2, \hat{\phi}_2), \ldots, \mathbf{a}_R(\hat{\theta}_L, \hat{\phi}_L)] \\ \hat{\mathbf{B}}^{(2)} &= \mathbf{F}^T[\mathbf{a}_T^*(\hat{\vartheta}_1, \hat{\varphi}_1), \mathbf{a}_T^*(\hat{\vartheta}_2, \hat{\varphi}_2), \ldots, \mathbf{a}_T^*(\hat{\vartheta}_L, \hat{\varphi}_L)] \\ \hat{\mathbf{B}}^{(3)} &= \mathbf{B}^{(3)} = [\mathbf{g}(\hat{\tau}_1), \mathbf{g}(\hat{\tau}_2), \ldots, \mathbf{g}(\hat{\tau}_L)]. \end{aligned} \tag{22}$$

Considering the structure of the noiseless signal tensor $\tilde{\mathcal{Y}}$,

we vectorize $\tilde{\mathcal{Y}}$ as $\text{vec}(\tilde{\mathcal{Y}})$, then the path gains $\hat{\boldsymbol{\alpha}} = [\hat{\alpha}_1, \hat{\alpha}_2, \ldots, \hat{\alpha}_L]^T$ can be estimated by

$$\hat{\boldsymbol{\alpha}} = (\hat{\mathbf{B}}^{(3)} \odot \hat{\mathbf{B}}^{(2)} \odot \hat{\mathbf{B}}^{(1)})^{\dagger} \text{vec}(\tilde{\mathcal{Y}}). \tag{23}$$

B. Improved Angle Estimation Method

The computational complexity of the 2-D search method in (21) is too high. If $\mathbf{F}$ and $\mathbf{W}$ have Kronecker structure, such structure will exist in columns of $\mathbf{A}^{(1)}$, $\mathbf{A}^{(2)}$, $\mathbf{B}^{(1)}$, and $\mathbf{B}^{(2)}$. For the lth column of $\mathbf{B}^{(1)}$ and $\mathbf{B}^{(2)}$, we reshape $\mathbf{b}_l^{(1)}$ and $\mathbf{b}_l^{(2)}$ to matrices by the inverse vectorization operation and obtain $\text{invec}(\mathbf{b}_l^{(1)}) \in \mathbb{C}^{I_1 \times I_2}$ and $\text{invec}(\mathbf{b}_l^{(2)}) \in \mathbb{C}^{J_1 \times J_2}$. By using the rank-1 truncated SVD, we have

$$\begin{aligned} \text{invec}(\mathbf{b}_l^{(1)}) &= \mathbf{u}_{1,l}\sigma_{1,l}\mathbf{v}_{1,l}^H \\ \text{invec}(\mathbf{b}_l^{(2)}) &= \mathbf{u}_{2,l}\sigma_{2,l}\mathbf{v}_{2,l}^H \end{aligned} \tag{24}$$

where $\sigma_{1,l}$ and $\sigma_{2,l}$ are the largest singular values, $\mathbf{u}_{1,l} \in \mathbb{C}^{I_1 \times 1}$, $\mathbf{v}_{1,l} \in \mathbb{C}^{I_2 \times 1}$, $\mathbf{u}_{2,l} \in \mathbb{C}^{J_1 \times 1}$, and $\mathbf{v}_{2,l} \in \mathbb{C}^{J_2 \times 1}$ are singular vectors corresponding to $\sigma_{1,l}$ and $\sigma_{2,l}$. Again the scaling ambiguity is removed by normalization operations. Then solving (21) can be replaced by several 1-D correlation-based methods as

$$\begin{aligned} \hat{\phi}_l &= \underset{\phi_l}{\text{argmax}} \frac{|\mathbf{v}_{1,l}^T \tilde{\mathbf{a}}_{Rz}(\phi_l)|}{\|\tilde{\mathbf{a}}_{Rz}(\phi_l)\|_2}, \hat{\theta}_l = \underset{\theta_l}{\text{argmax}} \frac{|\mathbf{u}_{1,l}^H \tilde{\mathbf{a}}_{Ry}(\theta_l, \hat{\phi}_l)|}{\|\tilde{\mathbf{a}}_{Ry}(\theta_l, \hat{\phi}_l)\|_2}, \\ \hat{\varphi}_l &= \underset{\varphi_l}{\text{argmax}} \frac{|\mathbf{v}_{2,l}^T \tilde{\mathbf{a}}_{Tz}(\varphi_l)|}{\|\tilde{\mathbf{a}}_{Tz}(\varphi_l)\|_2}, \hat{\vartheta}_l = \underset{\vartheta_l}{\text{argmax}} \frac{|\mathbf{u}_{2,l}^H \tilde{\mathbf{a}}_{Ty}(\vartheta_l, \hat{\varphi}_l)|}{\|\tilde{\mathbf{a}}_{Ty}(\vartheta_l, \hat{\varphi}_l)\|_2}. \end{aligned} \tag{25}$$

The 1-D search method will decrease the computational complexity from $\mathcal{O}(G^2)$ to $\mathcal{O}(G)$, where G denotes the number of angle grids in searching. However, the cumulative errors caused by the estimated elevation angles to estimate the azimuth angles also reduce the estimation accuracy. The NMS algorithm is also used to refine the results.

The proposed tensor-based channel estimation algorithm is summarized in Algorithm 1.

C. Channel Path Number Estimation

Most channel estimation algorithms suppose prior information on the number of paths. The fact is that it is unknown for the practical system. Considering $(\mathbf{A}^{(J_0,3)} \odot \mathbf{A}^{(2)})$ and $(\mathbf{A}^{(I_0,3)} \odot \mathbf{A}^{(1)})$ are of full column rank L generically, the rank of $\tilde{\mathbf{Y}}^s$ is equal to L [12]. If we know the rank of $\tilde{\mathbf{Y}}^s$, the channel path number can be decided correspondingly. Then a singular value hard thresholding (SVHT) method is proposed to estimate the channel path number.

Algorithm 1 Tensor-based channel estimation algorithm

1: **Input:** The received signal tensor $\mathcal{Y}$.
2: Rearrange $\mathcal{Y}$ as $\mathbf{Y}^s$ by spatial smoothing.
3: Calculate the truncated SVD of $\mathbf{Y}^s$, choose $\mathbf{U}_1$ and $\mathbf{U}_2$.
4: Calculate the EVD of $\tilde{\mathbf{Z}}$ by (17).
5: Estimate $\{\hat{\tau}_l\}_{l=1}^L$ and reconstruct $\mathbf{B}^{(3)}$.
6: Reconstruct $\mathbf{B}^{(2)}$ and $\mathbf{B}^{(1)}$ by (19) and (20).
7: Estimate the AoAs and AoDs $\{\hat{\theta}_l, \hat{\phi}_l, \hat{\vartheta}_l, \hat{\varphi}_l\}_{l=1}^L$ by 2-D search method (21) or improved 1-D search method (25) and refine them by the NMS algorithm.
8: Estimate the path gains $\{\hat{\alpha}_l\}_{l=1}^L$ by (23).
9: **Output:** Channel parameters $\{\hat{\alpha}_l, \hat{\theta}_l, \hat{\phi}_l, \hat{\vartheta}_l, \hat{\varphi}_l, \hat{\tau}_l\}_{l=1}^L$ and channel matrices $\{\hat{\mathbf{H}}_k\}_{k=0}^{K-1}$.

By sorting the singular values of $\tilde{\mathbf{Y}}^s$ in descending order, we aim to identify a hard threshold that discriminates the valid channel path against the noise. For $\tilde{\mathbf{Y}}^s$, let $\beta = \min(J_0 N_X, I_0 N_Y)/\max(J_0 N_X, I_0 N_Y)$, the optimal hard threshold coefficient is given by [14]

$$\rho_*(\beta) = \sqrt{2(\beta+1) + \frac{8\beta}{(\beta+1) + \sqrt{\beta^2 + 14\beta + 1}}}. \tag{26}$$

Thus the hard threshold is expressed as

$$\delta_*(\beta, \tilde{\mathbf{Y}}^s) = \frac{\rho_*(\beta)}{\sqrt{\mu_\beta}} \sigma_{med} \tag{27}$$

where σ_{med} is the median of the singular values of $\tilde{\mathbf{Y}}^s$ and μ_β denotes the median of the Marčenko-Pastur distribution. Let $\beta_\pm = (1 \pm \sqrt{\beta})^2$, μ_β is the unique solution to $\int_{\beta_-}^{\mu} \frac{\sqrt{(\beta_+ - x)(x - \beta_-)}}{2\pi\beta x} dx = \frac{1}{2}, \quad \beta_- \leq \mu \leq \beta_+$. Then the number of paths can be estimated by counting the number of the singular values of $\tilde{\mathbf{Y}}^s$ that are larger than $\delta_*(\beta, \tilde{\mathbf{Y}}^s)$.

IV. SIMULATION RESULTS

In our simulation, a non-line-of-sight (NLoS) condition is considered. The numbers of Rx antennas, Tx antennas, and RF chains of Rx are set to $N = 64 (N_1 = 8, N_2 = 8)$, $M = 64 (M_1 = 8, M_2 = 8)$ and $N_{RF} = 4$, respectively. The lengths of the pilot sequence at the Tx and Rx are set to $N_X = 28$ and $N_Y = 28$ associated with $J_1 = 7, J_2 = 4$ and $I_1 = 7, I_2 = 4$. The channel bandwidth and the number of subcarriers are assumed to be 100 MHz and $K = 64$, respectively. The number of paths is set to $L = 5$. The channel complex gain α_l follows the i.i.d $\mathcal{CN}(0, 1)$. The azimuth angles of the AoAs and AoDs $\{\theta_l, \vartheta_l\}$ and the elevation angles of the AoAs and AoDs $\{\phi_l, \varphi_l\}$ are uniformly distributed in $(-\frac{\pi}{2}, \frac{\pi}{2})$ and $(0, \pi)$. Each path's normalized delay τ_l is uniformly chosen from [0,20], corresponding to a range of 0∼0.2μs.

We first evaluate the probability of correct path estimation of three methods, i.e., the SVHT method, the minimum description length (MDL) method, and the generalized N-D MDL method [15]. Fig. 2 and Fig. 3 show that the SVHT method performs much better than the other two methods at low SNRs and many paths. The reason is that the SVHT method fully considers the row-to-column ratio of the signal matrix and accurately estimates the noise level. With the SNR increasing, the SVHT method reaches probability one of correct estimation faster than the other two methods. When the number of paths increases, the SVHT method is almost unaffected, while the other two methods worsen significantly.

Then the performance of the proposed algorithm is investigated by the normalized mean square error (NMSE), i.e., $\text{NMSE} = \frac{\sum_{k=0}^{K-1} \|\mathbf{H}_k - \hat{\mathbf{H}}_k\|_F^2}{\sum_{k=0}^{K-1} \|\mathbf{H}_k\|_F^2}$, where $\hat{\mathbf{H}}_k$ is constructed by the estimated channel parameters. As shown in Fig. 4, the NMSE of the proposed algorithm is always smaller than that of the SAGE-based algorithm [3], the beamspace ESPRIT algorithm [6], and the TTVCPD algorithm [7], which is partly due to the truncated SVD eliminates the impact of noise. The performances of the improved 1-D search method are close to that of the 2-D search method. The 1-D search method can effectively reduce computational complexity with a slight sacrifice of estimation accuracy. The performances of

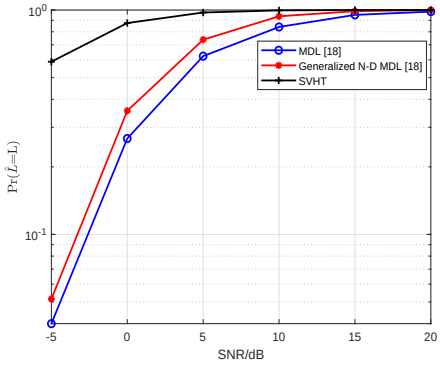

Fig. 2. Probability of correct estimation versus different SNRs.

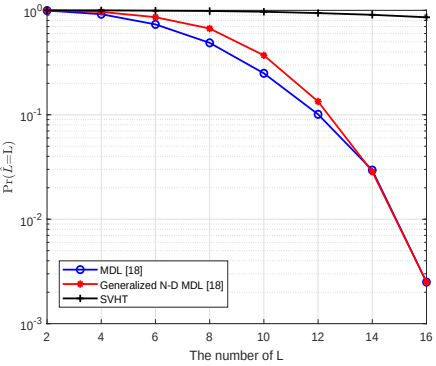

Fig. 3. Probability of correct estimation versus different numbers of paths (SNR = 10 dB).

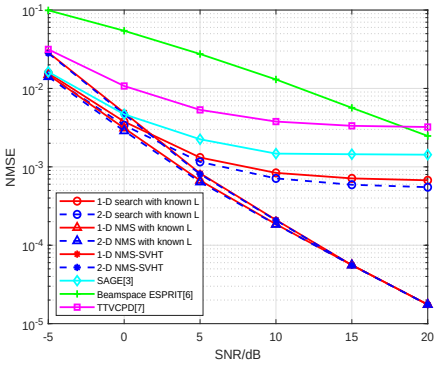

Fig. 4. NMSE versus different SNRs.

the 1-D search followed by the NMS refinement (1-D NMS) method and 2-D search followed by the NMS refinement (2-D NMS) method are better than that of the initial 1-D search method and 2-D search method at both low and high SNRs. The performance advantages diminish when the SNR becomes lower because the optimization ability of the NMS algorithm decreases. When the number of paths is unknown and estimated by the SVHT method, its NMSE is also shown in Fig. 4. The performances of the 1-D NMS-SVHT and 2-D NMS-SVHT methods are the same as those of the 1-D NMS and 2-D NMS methods with known L at high SNRs. When the SNR is low, the SVHT method may miss paths with low signal energy, which leads to estimation errors.

V. CONCLUSIONS

This letter proposes a tensor-based channel parameters estimation scheme for channel sounding with a mmWave 3-D massive MIMO-OFDM system with UPA antennas. A simple algebra-based method has been used to conduct CP decomposition. The AoAs and AoDs have been estimated by the 2-D search method or the improved 1-D search method, with the latter capable of effectively reducing the computational complexity, and then refined by the NMS algorithm. We have also proposed an SVHT method to estimate the unknown path numbers, realizing joint estimation of path number and channel parameters. Simulation results have shown that the proposed algorithm and the SVHT method can achieve high estimation accuracy. The effect of the antenna radiation pattern is essential and has not been considered in this letter. We will explore and extend the algorithm's capability in the future.

APPENDIX A
PROPERTIES OF THE KHATRI-RAO PRODUCT AND KRONECKER PRODUCT

The following properties of the Khatri-Rao product and Kronecker product are used in this letter:

$$(\mathbf{A}\otimes\mathbf{B})(\mathbf{C}\otimes\mathbf{D}) = \mathbf{AC}\otimes\mathbf{BD} \tag{A.1}$$
$$(\mathbf{A}\otimes\mathbf{B})(\mathbf{C}\odot\mathbf{D}) = \mathbf{AC}\odot\mathbf{BD} \tag{A.2}$$
$$(\mathbf{A}\odot\mathbf{B})\mathbf{\Delta} = \mathbf{A}\odot(\mathbf{B\Delta}) = (\mathbf{A\Delta})\odot\mathbf{B} \tag{A.3}$$
$$(\mathbf{A}\odot\mathbf{B})\mathbf{\Pi} = (\mathbf{A\Pi})\odot(\mathbf{B\Pi}) \tag{A.4}$$

where $\mathbf{\Delta}$ is a diagonal matrix and $\mathbf{\Pi}$ is a permutation matrix.

REFERENCES

[1] C.-X. Wang et al., "On the road to 6G: Visions, requirements, key technologies, and testbeds," *IEEE Commun. Surveys. Tuts.*, vol. 25, no. 2, pp. 905–974, 2nd Quart., 2023.

[2] S. A. Busari, K. M. S. Huq, S. Mumtaz, L. Dai and J. Rodriguez, "Millimeter-wave massive MIMO communication for future wireless systems: A survey," *IEEE Commun. Surveys. Tuts.*, vol. 20, no. 2, pp. 836-869, 2nd Quart., 2018.

[3] C. Liu, J. Sun, W. Zhang, and C.-X. Wang, "A new SAGE-based channel estimation scheme for millimeter wave MIMO-OFDM systems with hybrid beamforming techniques," in *Proc. IEEE/CIC'22*, Foshan, China, pp. 844–849, Aug. 2022.

[4] M. Ke, Z. Gao, Y. Wu, X. Gao, and R. Schober, "Compressive sensing-based adaptive active user detection and channel estimation: Massive access meets massive MIMO," *IEEE Trans. Signal Process.*, vol. 68, pp. 764–779, Jan. 2020.

[5] Z. Zhou, J. Fang, L. Yang, H. Li, Z. Chen, and R. S. Blum, "Low-rank tensor decomposition-aided channel estimation for millimeter wave MIMO-OFDM systems," *IEEE J. Sel. Areas Commun.*, vol. 35, no. 7, pp. 1524–1538, Jul. 2017.

[6] F. Wen, N. Garcia, J. Kulmer, K. Witrisal, and H. Wymeersch, "Tensor decomposition based beamspace ESPRIT for millimeter wave MIMO channel estimation," in *Proc. IEEE Global. Commun. Conf.*, Abu Dhabi, United Arab Emirates, pp. 1–7, Dec. 2018.

[7] X. Gong, W. Chen, L. Sun, J. Chen, and B. Ai, "An ESPRIT-based supervised channel estimation method using tensor train decomposition for mmWave 3-D MIMO-OFDM systems," *IEEE Trans. Signal Process.*, vol. 71, pp. 555–570, Feb. 2023.

[8] J. Hong, J. Wang, C. Liu, J. Sun, W. Zhang, and C.-X. Wang, "A tensor-based high resolution millimeter wave massive MIMO channel parameters estimation scheme," in *Proc. IEEE Int. Conf. Commun. (ICC)*, Rome, Italy, pp. 5060–5065, Jun. 2023.

[9] R. W. Heath, N. González-Prelcic, S. Rangan, W. Roh, and A. M. Sayeed, "An overview of signal processing techniques for millimeter wave MIMO systems," *IEEE J. Sel. Topics Signal Process.*, vol. 10, no. 3, pp. 436–453, Apr. 2016.

[10] T. G. Kolda and B. W. Bader, "Tensor decompositions and applications," *SIAM Rev.*, vol. 51, no. 3, pp. 455–500, Aug. 2009.

[11] J. Wang, W. Zhang, Y. Chen, Z. Liu, J. Sun, and C.-X. Wang, "Time-varying channel estimation scheme for uplink MU-MIMO in 6G systems," *IEEE Trans. Veh. Technol.*, vol. 71, no. 11, pp. 11820–11831, Nov. 2022.

[12] M. Sørensen and L. D. Lathauwer, "Blind signal separation via tensor decomposition with vandermonde factor: Canonical polyadic decomposition," *IEEE Trans. Signal Process.*, vol. 61, no. 22, pp. 5507–5519, Nov. 2013.

[13] J. C. Lagarias, J. A. Reeds, M. H. Wright, and P. E. Wright, "Convergence properties of the Nelder-Mead simplex method in low dimensions," *SIAM J. Optim.*, vol. 9, no. 1, pp. 112–147, Jan. 1998.

[14] M. Gavish and D. L. Donoho, "The optimal hard threshold for singular values is $4/\sqrt{3}$," *IEEE Trans. Inf. Theory*, vol. 60, no. 8, pp. 5040–5053, Aug. 2014.

[15] K. Liu, J. P. C. L. da Costa, H. C. So, L. Huang, and J. Ye, "Detection of number of components in CANDECOMP/PARAFAC models via minimum description length," *Digit. Signal Process.*, vol. 51, pp. 110–123, Apr. 2016.